catalysts

MDPI

Article

Minimally Invasive Glucose Monitoring Using a Highly Porous Gold Microneedles-Based Biosensor: Characterization and Application in Artificial Interstitial Fluid

Paolo Bollella [1], Sanjiv Sharma [2], Anthony E. G. Cass [3], Federico Tasca [4] and Riccarda Antiochia [5,*]

1 Department of Chemistry and Biomolecular Science, Clarkson University, Potsdam, NY 13699, USA
2 College of Engineering, Swansea University, Swansea SA1 8EN, Wales, UK
3 Department of Chemistry & Institute of Biomedical Engineering, Imperial College, London W12 OBZ, UK
4 Departamento de Quimica de los Materiales, Universidad de Santiago de Chile, 8320000 Santiago, Chile
5 Department of Chemistry and Drug Technologies, Sapienza University of Rome, 00185 Rome, Italy
* Correspondence: riccarda.antiochia@uniroma1.it; Tel.: +39-06-49913906

Received: 28 May 2019; Accepted: 20 June 2019; Published: 30 June 2019

Abstract: In this paper, we present the first highly porous gold (h-PG) microneedles-based second-generation biosensor for minimally invasive monitoring of glucose in artificial interstitial fluid (ISF). A highly porous microneedles-based electrode was prepared by a simple electrochemical self-templating method that involves two steps, gold electrodeposition and hydrogen bubbling at the electrode, which were realized by applying a potential of −2 V versus a saturated calomel electrode (SCE). The highly porous gold surface of the microneedles was modified by immobilization of 6-(ferrocenyl)hexanethiol (FcSH) as a redox mediator and subsequently by immobilization of a flavin adenine dinucleotide glucose dehydrogenase (FAD-GDH) enzyme using a drop-casting method. The microneedles-based FcSH/FAD-GDH biosensor allows for the detection of glucose in artificial interstitial fluid with an extended linear range (0.1–10 mM), high sensitivity (50.86 μA cm^{-2} mM^{-1}), stability (20% signal loss after 30 days), selectivity (only ascorbic acid showed a response about 10% of glucose signal), and a short response time (3 s). These properties were favourably compared to other microneedles-based glucose biosensors reported in the literature. Finally, the microneedle-arrays-based second-generation biosensor for glucose detection was tested in artificial interstitial fluid opportunely spiked with different concentrations of glucose (simulating healthy physiological conditions while fasting and after lunch) and by placing the electrode into a simulated chitosan/agarose hydrogel skin model embedded in the artificial ISF (continuous glucose monitoring). The obtained current signals had a lag-time of about 2 min compared to the experiments in solution, but they fit perfectly into the linearity range of the biosensor (0.1–10 mM). These promising results show that the proposed h-PG microneedles-based sensor could be used as a wearable, disposable, user-friendly, and automated diagnostic tool for diabetes patients.

Keywords: microneedles; porous gold; glucose; interstitial fluid; minimally invasive

1. Introduction

Optimal diabetes management requires accurate real-time monitoring of glucose. People with diabetes have to test their blood sugar level several times every day to know how different foods, medications, and activities may affect it [1,2]. The normal blood glucose level (tested while fasting) for non-diabetics should be between 3.9 and 7.1 mmol/L (70–130 mg/dL). The mean normal blood glucose

level in humans is about 5.5 mmol/L. However, this level fluctuates throughout the day. The common method for monitoring glucose concentrations involves sampling of a small amount of blood, usually from a fingertip, using a lancet that lightly pricks the skin, with discomfort for the patient, especially in children or elderly people. Several commercial glucose meters based on amperometric electrochemical technology have been realized to help patients manage blood glucose routine testing; however, they provide just a single glucose reading and require repeated finger pricks [3,4].

In order to avoid this problem, commercially available glucose monitoring devices (CGMs) have been developed that can provide real time, dynamic glucose information every five minutes [5]. The sensor is placed just under the skin and can be used for up to 10 days, requiring patients to remove and reinsert a new sensor into subcutaneous tissue in another part of the body [6]. They are based on glucose oxidase (GOx) and continuously measure glucose levels in the interstitial fluid (ISF) using a needle that penetrates into the subcutaneous tissue. Glucose concentrations in capillary bloods are the same as in the ISF with a mean lag time of 6–7 min [7–9]. CGM devices offer the advantage of being wearable biosensors that send data wirelessly to a display device through a transmitter. Despite their advantages, these devices are still invasive and associated with some discomfort. Moreover, they show biofouling effects due to surface deposition of proteins and cells [7].

Amperometric biosensors based on microneedles technology represent an interesting compromise [8–10]. Like the CGM devices, microneedles-based biosensors allow for the continuous monitoring of glucose in the ISF. However, thanks to their short length (1 mm), they can penetrate only the first layer of the human skin, the epidermis (thickness between 50 and 500 μm) without penetrating the second layer, the dermis (thickness in the range 500–2000 μm), unlike normal needles (6 mm in length). The dermis is the most vascularized region of the human skin, whereas no blood vessels nor nerve endings are present in the epidermis. According to these reasons, they are significantly less painful than CGSs, improving comfort and treatment quality in patients affected by diabetes [11–13]. Moreover, they show minimized biofouling effects as they are changed every day compared to other implantable devices that are changed every two weeks or more. Another important characteristic of the microneedles-based biosensors is their high sensitivity; they provide larger currents thanks to their larger electrode surface areas. Furthermore, they also showed high reproducibility during in vitro and in vivo experiments [5,9], as well as simplicity and low cost in terms of production. They also cause lower skin irritation and a lower risk of local infection and bleeding [14].

Microneedles-based devices were initially used as transdermal delivery systems of a number of drugs and other compounds [10,14–17]. Subsequently, they were utilized for the development of transdermal analytical sensors for pain-free detection of analytes of clinical relevance. Although most studies apply the microneedle arrays for the continuous monitoring of glucose [9,11,18–25], a few papers have also been published on the use of microneedles-based biosensors for the detection of other bioanalytes, such as lactate [9,23,26–28], alcohol [29], beta-lactams [30], and glutamate [31]. Glucose biosensors generally involve the detection of hydrogen peroxide produced by the reduction of oxygen catalyzed by a GOx reaction. Unfortunately, it is known that the oxidation of hydrogen peroxide occurs at a quite high overpotential at which other electroactive species can be oxidized [32,33]. The use of a redox mediator allows us to lower the detection potential of glucose, thus reducing the possible interferences with a consequent increase of the selectivity of the biosensor. Among the electroactive groups, ferrocene and its derivatives have been extensively used as model systems to study the reversible electron exchange between the mediator and gold electrodes, thanks to the simple and good electrochemical characteristics of the ferrocene group [34–36].

Highly porous gold electrodes (h-PG) have pores in the micrometer range that increase drastically the electrode surface area and the relative current densities [37,38]. Three main methods have been generally used to fabricate porous gold films: de-alloying, electrochemical deposition, and templating. De-alloying is a corrosive process of alloy components by selective dissolution of the most active element in the alloy, which is gold, which could be done either electrochemically or chemically. Electrochemical deposition is an electrodissolution–disproportion–deposition reaction between gold

and HCl [39]. The templating method combines various techniques, such as the flow-stream technique, sputter deposition, and electrochemical methods, and involves the following three steps: preparation of the template, deposition of gold, and removal of the template. The self-templating method is a simplified and time-saving templating method that involves only two steps: gold electrodeposition and gas bubbling as a self-template [38,40–42].

In this work, a highly porous gold (h-PG) microneedles-based biosensor for minimally invasive sensing of glucose in artificial interstitial fluid was realized and investigated. The h-PG surface was developed by electrodeposition of a gold layer followed by hydrogen bubbling at the electrode surface through applying a negative potential of −2 V versus a saturated calomel electrode (SCE) in a solution containing NH_4Cl as a supporting electrolyte and a hydrogen source. The h-PG microneedles were characterized and compared to microneedles modified with multiwalled carbon nanotubes (MWCNTs) and to a planar gold electrode before and after the modification with h-PG and MWCNTs. The flavin adenine dinucleotide glucose dehydrogenase (FAD-GDH)/6-(ferrocenyl)hexanethiol (FcSH)/h-PG microneedles-based electrode was successfully realized by immobilization of the redox mediator 6-(ferrocenyl)hexanethiol and the FAD-GDH enzyme [43]. An image of the microneedles and a schematic representation of the as-assembled microneedles-based electrode are reported in Figure 1A,B, respectively. To the best of our knowledge, this is the first example of a h-PG-modified microneedles-based electrode reported in the literature. Finally, the feasibility of the developed biosensor for minimally invasive monitoring of glucose was evaluated in artificial interstitial fluid and in a simulated skin model.

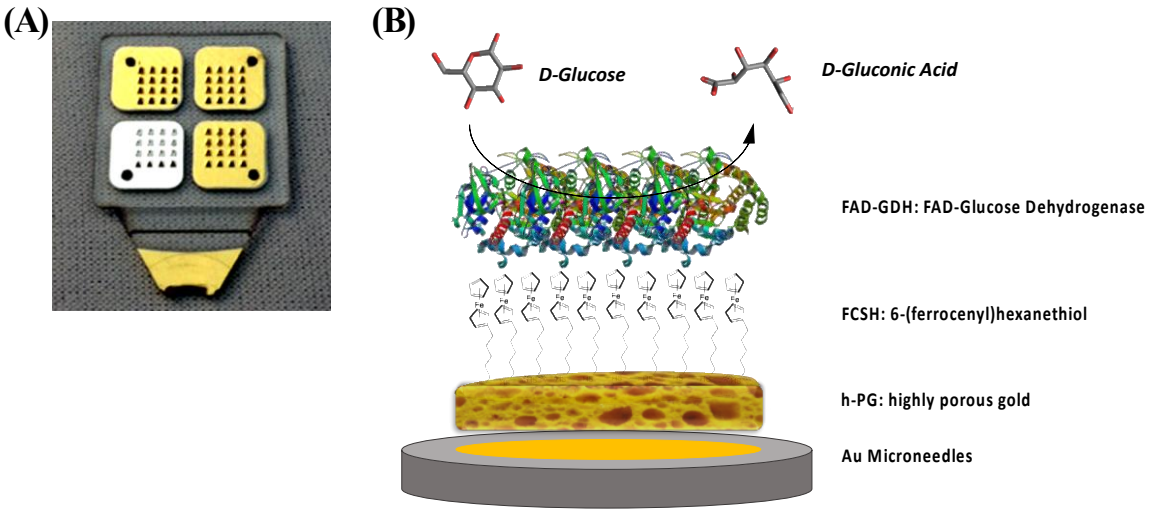

Figure 1. (**A**) Photo of four 4 × 4 microneedle arrays metallized with gold and silver; (**B**) Schematic representation of the highly porous gold (h-PG)/6-(ferrocenyl)hexanethiol (FcSH)/flavin adenine dinucleotide glucose dehydrogenase (FAD-GDH)/Au microneedles-based glucose biosensor. Figure 1A is reproduced from ref. [28] with permission of Elsevier Science ltd (2019).

2. Results and Discussion

2.1. SEM and Electrochemical Characterization of h-PG/Au Microneedles Electrodes

SEM experiments were carried out to investigate the morphology of the highly porous gold microneedles-based electrode. SEM images of the bare and the h-PG-modified microneedles-based electrode are presented in Figures 2A and 2B (mag. ×100 and mag. ×1000) and 2C (mag. ×1000), respectively. It is possible to note the well-defined pores with diameters of approximately 25 µm, as shown in Figure 2C. The highly porous gold surface is probably obtained by the reduction of Au^{3+} ions to Au^0 atoms with their subsequent aggregation and deposition on the rough surface of the microneedles electrode to form the porous structure. A key point of the fabrication of the porous surface is the choice of a suitable negative potential and the right time at which to apply it. A negative

potential of −3 V generated hydrogen bubbling at the microneedles surface of the working electrode that was too vigorous and destroyed the gold surface. A lower potential (about 0 V) was not enough to generate the proper hydrogen bubbling to create the porous structure. The potential of −2 V was therefore chosen as a compromise to guarantee a sufficient bubbling of hydrogen at the gold surface to create the proper porous structure without ruining the surface itself. A time of 60 s was chosen as it is the length of time that enabled the porous structure to entirely cover the electrode. Another important parameter that was carefully optimized was the distance between the bottom of the microneedle arrays structure and the beaker's bottom. The highly porous gold surface was produced when this gap was not greater than 3 mm, probably because a larger distance would not facilitate the diffusion processes of H^+, $AuCl_4$, and Cl^- ions towards and away from the electrode surface to enable the aggregation and deposition of the gold atoms on the electrode surface to form the porous structure [44].

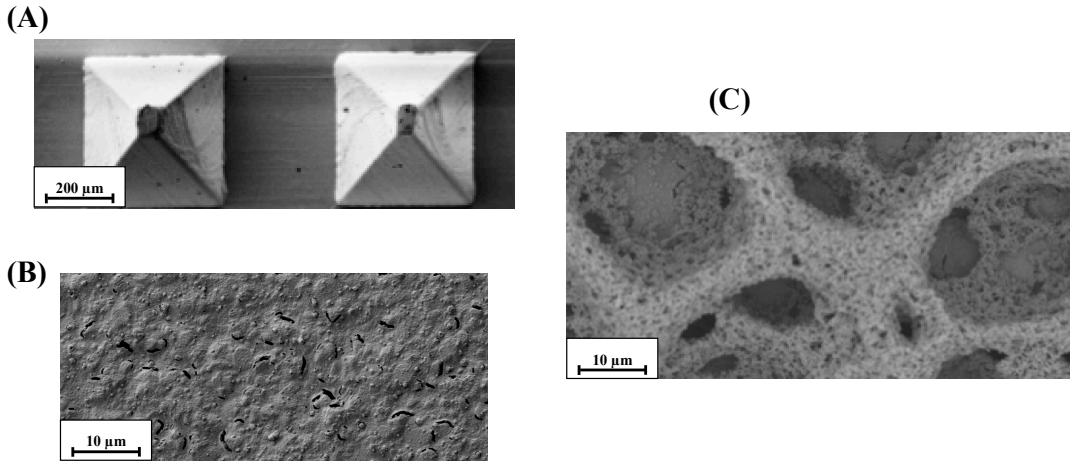

Figure 2. SEM images of (**A**,**B**) a bare microneedles gold electrode and (**C**) an h-PG microneedles gold electrode with different magnifications. (**A**) 6.00 kV, mag. ×100; (**B**,**C**) 10.0 kV, mag. ×1000.

In order to demonstrate the improvements in the electrodeposition method in terms of electroactive area, the gold film was characterized electrochemically in 0.5 M H_2SO_4 at a scan rate of 100 mV s^{-1}. The cyclic voltammogram shows two anodic peaks due to gold oxidation starting at about 1 V versus SCE and one large cathodic peak at about 0.7 V versus SCE due to the reduction of the gold oxide formed during the positive sweep, as shown in Figure 3A. The real surface area of the highly porous gold electrode was calculated by integrating the charge required for reducing the gold oxide (Figure 3A, red curve), and the results were compared with those obtained with a bare microneedles gold electrode with the same geometric surface (Figure 3A, black curve). The h-PG microneedles electrode showed a real surface area of 88.50 cm^2, assuming that the charge density for the reduction of gold oxide is 390 µC cm^{-2}, a value that is about 100 times higher compared to the bare microneedles gold electrode (0.90 ± 0.02 cm^2).

The real active area of the porous surface was also investigated by cyclic voltammetry in a solution of $Fe(CN)_6^{3-/4-}$ (Figure 3B,C). A remarkable enhancement of the anodic and cathodic peak current densities after the h-PG electrodeposition was observed as a consequence of the increase in the electroactive surface area. By comparing these results with those obtained with a planar gold electrode before and after the h-PG electrodeposition, it can be easily noted that the increase in the current after the h-PG electrodeposition is larger in the case of the Au-microneedles electrode (Figure 3B) compared to the Au-planar electrode (Figure 3C). The roughness factors of the two electrodes before and after the electrodeposition of h-PG have been calculated, and the roughness factor after the electrodeposition of h-PG resulted to be almost 20 times higher in the case of the microneedles electrode (ρ = 1032.1 ± 2.3) compared to the planar electrode (ρ = 56.0 ± 0.8) (Table S1). The particular geometry of the microneedles probably allows for a better electrodeposition of h-PG and therefore a larger electroactive surface area is obtained. Table S1 also shows the electroactive area and roughness factor of

the microneedles and planar gold electrodes modified by electrodeposition of Au-MWCNTs, according to a procedure reported in our previous work [29], for comparison. It is interesting to note the large enhancement of the roughness factor in the case of the h-PG microneedles-based electrode, which results to be three times higher than that obtained with microneedles modified with Au-MWCNTs (Figure 3B,C, blue curves). The heterogeneous electron transfer rate constants (k^0, cm s^{-1}) for the planar gold and the microneedle gold electrodes before and after the modification with h-PG and Au-MWCNTs are also reported in Table S1, calculated with a method proposed by Lavagnini et al. that merges the Klingler–Kochi and Nicholson and Shain methods developed for irreversible and reversible systems, respectively [45,46]. The Au microneedles/h-PG electrode showed the highest k_0 value ($k_0 = 56.2 \pm 0.5 \times 10^3$ cm s^{-1}), attesting to faster electron transfer kinetics.

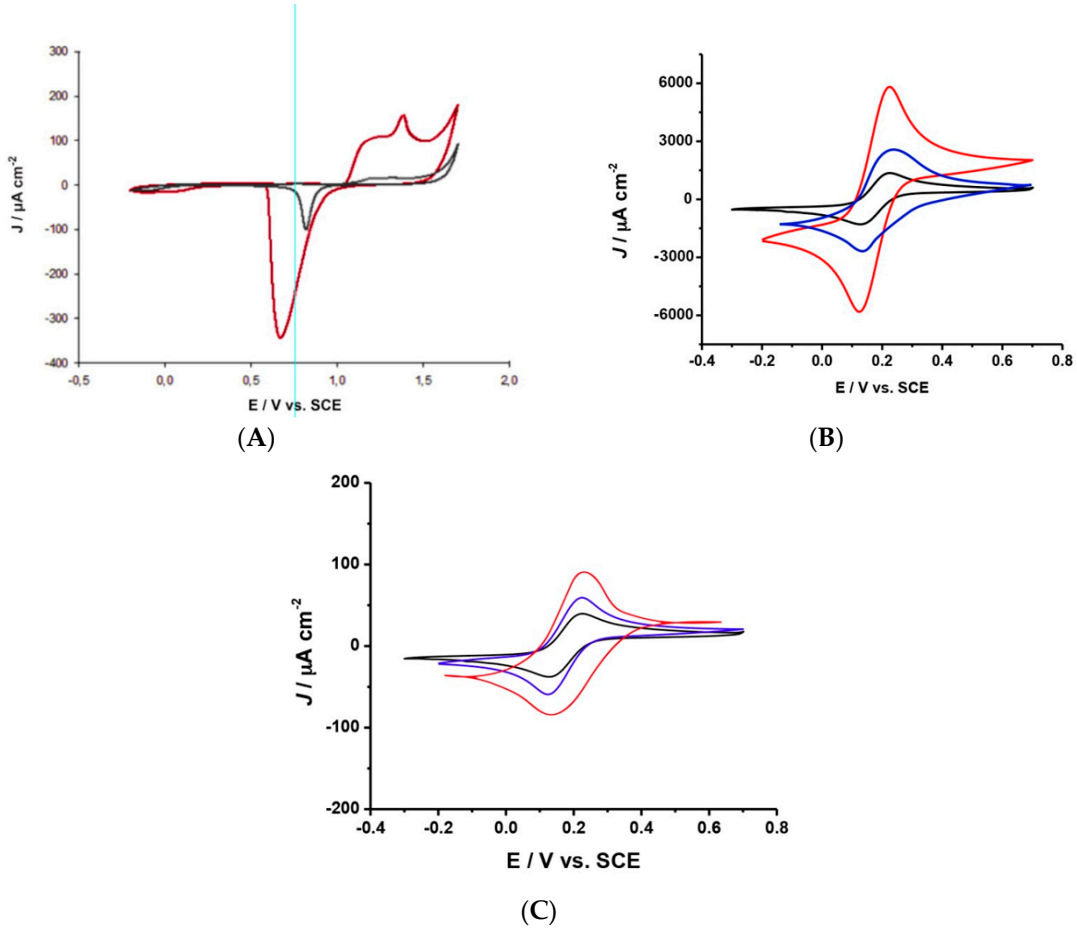

Figure 3. Cyclic voltammograms of: (**A**) the h-PG/Au microneedles electrode (red curve) and the bare Au/microneedles electrode (black curve) in H_2SO_4 0.5 M, v = 100 mV $^{s-1}$; Au microneedles (**B**) and the Au planar electrode (**C**) unmodified (black) and after the electrodeposition of h-PG (red curves) and Au-multiwalled carbon nanotubes (MWCNTs) (blue curves) in 5 mM $Fe(CN)_6^{3-/4-}$, 50 mM phosphate-buffered saline (PBS) at pH 7.5, and 137 mM NaCl, v = 50 mV s^{-1}, T = 25 °C.

2.2. Electrochemical Characterization of FcSH/h-PG/Au Microneedles Electrodes

The h-PG/Au microneedles-based electrode was subsequently modified by deposition of the redox mediator 6-(ferrycenyl)hexanethiol (Fc-SH), by keeping the electrode overnight in a solution of 8 mM FcSH in phosphate buffer at pH 7.5. The voltammetric profile of the modified electrodes shows a couple of quasi reversible redox peaks, as shown in Figure 4, at different scan rates. It is interesting to note that the voltammograms show the typical shape of a surface-bound species with a small separation between the anodic and cathodic peaks. The formal redox potential of FcSH was determined to be about +0.38 V versus SCE, in good agreement with the value reported in the literature for this

mediator [47]. An analysis of the Faradaic current as a function of v resulted in a linear relationship, as shown in the inset of Figure 4, attesting to the typical dependence of the current on the scan rate of a surface-confined mediator.

The effect of FcSH amount was investigated and the maximum current signal was obtained by using an 8 mM FcSH solution for the mediator immobilization (data not shown). Higher amounts of FcSH showed a decrease in current response, probably due to a steric hindrance effect of the mediator on the microneedles electrode surface [48,49].

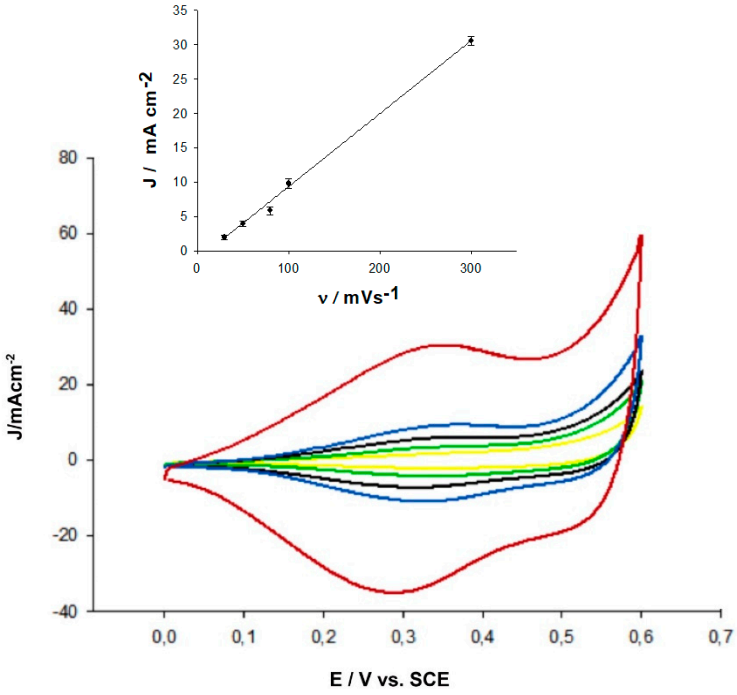

Figure 4. Cyclic voltammograms obtained with a FcSH/h-PG/Au microneedles electrode at different scan rates: 30 mVs^{-1} (yellow); 50 mVs^{-1} (green); 80 mVs^{-1} (black); 100 mVs^{-1} (blue); and 300 mVs^{-1} (red) in 50 mM PBS at pH 7.5. In the inset: the dependence of J on v relative to the different curves.

2.3. Application of the h-PG/Au Microneedles-Based Glucose Biosensor in Artificial ISF

Before studying the amperometric responses toward D-glucose of the assembled FAD-GDH/FcSH/h-PG/Au microneedles-based glucose biosensor, the amount of loaded enzyme was carefully examined and optimized by drop-casting onto the microneedles surface FAD-GDH amounts varying from 1 to 5 U. The variations in the current densities as a function of the enzyme loading are shown in Figure S1. The biosensor response increased proportionally with the enzyme loading up to 1.5 U, corresponding to 5 µL of enzyme. A slight decline in the response signal is observed at higher enzyme concentrations probably due to the rigid structure of the FcSH molecule, showing a rate-limiting dependence on the enzyme concentration only at low loaded FAD-GDH amounts. Therefore, 1.5 U was the concentration of enzyme utilized for the biosensor's development.

Figure 5A shows a comparative cyclic voltammogram of the FAD-GDH/FcSH/h-PG microneedles-based electrode in the absence and in the presence of glucose in artificial interstitial fluid. A good electrocatalytic current was registered with an onset potential of +35 mV, in agreement with the value reported in the literature for the redox potential of the FcSH mediator (E_0 = +38 mV vs. SCE).

In Figure 5B, it is possible to observe that the calibration curve for glucose detection in artificial interstitial fluid has an extended linear range between 0.1 and 10 mM glucose (inset Figure 5B) and a sensitivity of 50.86 µA cm^{-2} mM^{-1} (R^2 = 0.97, n = 5). The detection limit resulted to be 50 µM, calculated using the relation 3σ/S, with σ and S the absolute standard deviation of the intercept and the slope of the calibration curve, respectively. By fitting the calibration curve to the Michaelis–Menten

kinetic parameters, a J_{max} value of 520.20 ± 25.11 μA cm^{-2} was obtained and a Michaelis–Menten constant (K_M) of 11.75 ± 1.18 mM was calculated, showing a good affinity of the FAD-GDH enzyme for glucose.

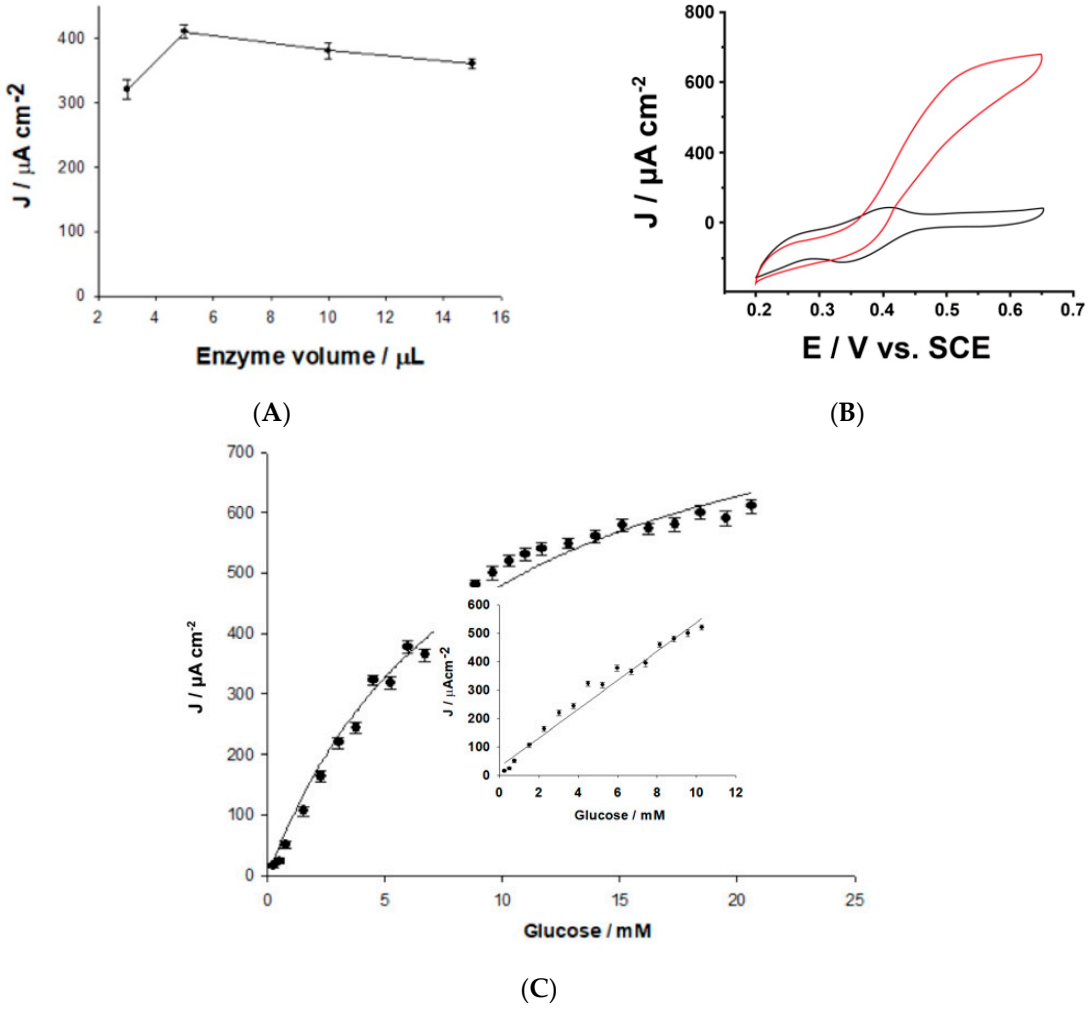

Figure 5. (**A**) Effect of enzyme loading on biosensor response; (**B**) Cyclic voltammogram of the FAD-GDH/FcSH/h-PG microneedles-based electrode in the absence and in the presence of glucose; (**C**) The calibration curve of the glucose biosensor; inset: linear range. Experimental conditions: artificial interstitial fluid (ISF) pH 7.5; E = 0.5 V versus SCE.

2.4. Effect of pH and Temperature on the Stability and Selectivity of the Glucose Biosensor

The median pH and temperature values are important parameters for enzymes to maintain their activities and catalysis efficiency. The optimum pH and temperature values for the FAD-GDH enzyme in soluble form was found to be pH 7 and 35 °C, respectively [50]. A possible shift in optimal pH can be obtained for immobilized enzymes. The pH effect was studied by varying the pH of the ISF in the range between 3 and 9, using acetate, phosphate, and TRIS buffer. The maximum current responses were obtained in phosphate buffer pH 7.5 (Figure 6A) at 35 °C (Figure 6B). These results are of great consequence for a potential application of the microneedles-based biosensor under human physiological conditions.

An important requirement for a microneedles-based biosensor for transdermal analysis is the ability to operate over several days with no significant decrease in its response. The stability was examined using a 0.2 mM glucose solution over 30 days by using the biosensor in continuous operation for 10 measurements every day. A high stable current response was obtained over the whole period,

with a decrease in the initial signal response of about 20% after 30 days (Figure 6C). Such a high lifetime of the biosensor probably reflects the stability of the enzyme in the highly porous structure of the microneedles electrode surface.

Another important feature of a microneedles-based biosensor is the capacity to avoid interference from other electroactive compounds present in the human interstitial fluid. The response of the proposed biosensor was evaluated with a standard glucose concentration and with equal concentrations of exogenous interfering compounds, such as D-fructose, D-mannitol, D-galactose, and ascorbic acid. These compounds have a similar oxidation potential to glucose and could affect the biosensor's current response. Figure 6D shows the high selectivity of the proposed biosensor, as no tested compound showed any significant current signal with the exception of ascorbic acid, whose signal was, however, about 10% of the signal obtained for glucose. Also, xylose and maltose were tested, but they did not show any current signal, confirming the high selectivity of the proposed biosensor.

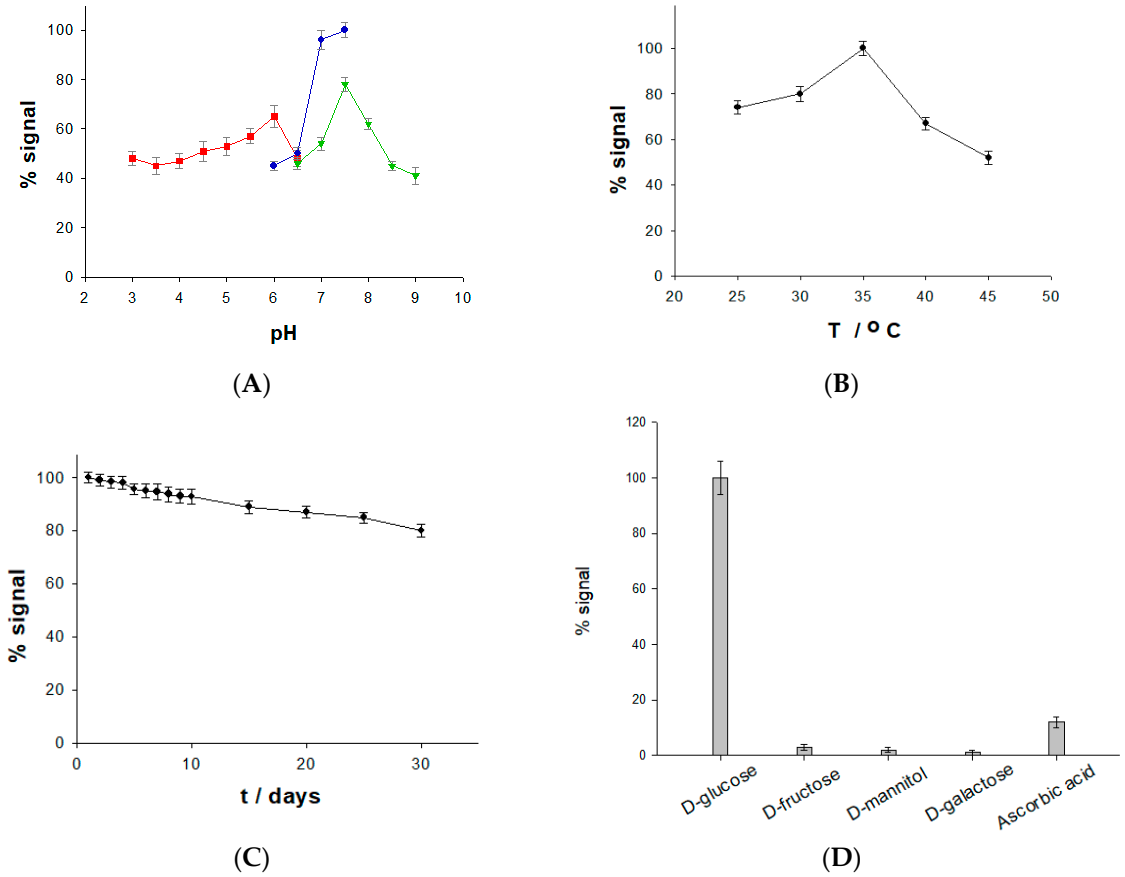

Figure 6. Effect of pH (**A**), temperature (**B**), stability (**C**), and the influence of interference (**D**) on the Au microneedles/h-PG/FcSH/FAD-GDH biosensor. Experimental conditions: (**A**) 0.1 M acetate buffer (red), 0.1 M phosphate buffer (blue), 0.1 M TRIS buffer (green), E° = 0.5 V versus SCE, 10 mM glucose; (**B**) and (**C**) phosphate buffer pH 7.5, E°= 0.5 V versus SCE, 10 mM glucose; (**D**) 20 µM glucose, 20 µM fructose, 20 µM mannitol, 20 µM galactose, 20 µM ascorbic acid, phosphate buffer pH 7.5, E°= 0.5 V versus SCE.

An analytical comparison with the results obtained with other microneedles-based glucose biosensors recently reported in the literature is shown in Tables 1 and 2. It is interesting to note that most microneedles-based biosensors show extended linear ranges and high sensitivities; however, they are based on the oxidation of H_2O_2 (first-generation biosensors), which occurs at high overpotentials with the obvious drawback of the possibility of side reactions, such as the oxidation of ascorbic acid, lactic acid, and uric acid, thus hampering the selectivity of the biosensor [51–55]. The second-generation FAD-GDH/FcSH/h-PG/Au microneedles-based biosensor proposed in this study exhibits a linear range

and a sensitivity comparable to the devices based on the "first generation" biosensor mechanism without the drawback of the high overpotential and the dependence on oxygen concentration, extremely important requirements for a subcutaneous biosensor, while maintaining at the same time a much larger linear range compared to the second-generation microneedles-based biosensor based on MWCNTs reported in the literature [23,56].

Table 1. Heterogeneous electron transfer rate constant (k_0), real electroactive area (A_{EA}), and roughnesss factor (ρ) of the gold planar electrode and the gold microneedles-based electrode before and after the electrodeposition of h-PG and Au-MWCNTs. A_{geo} planar Au electrode = 0.020 cm^2; A_{geo} microneedle electrode = 0.2 cm^2.

Electrode	$k_0/10^{-3}$ cm s^{-1}	A_{EA}/cm^2	ρ
Au planar electrode	1.1 ± 0.1	0.08 ± 0.01	4.0 ± 0.2
Au planar electrode/h-PG	3.0 ± 0.8	1.12 ± 0.02	56.0 ± 0.8
Au planar electrode/Au-MWCNTs	2.7 ± 0.9	1.24 ± 0.02	39.5 ± 0.6
Au microneedles	5.8 ± 0.2	2.02 ± 0.18	10.1 ± 0.6
Au microneedles/h-PG	56.2 ± 0.5	206.42 ± 0.42	1032.1 ± 2.3
Au microneedles/Au-MWCNTs	16.3 ± 0.4	60.36 ± 0.31	301.6 ± 1.6

Table 2. Comparison between different microneedles-based biosensors for glucose detection.

Microneedles Biosensor Platform	Detection Technique	Linear Range (mM)	Biosensor Type	Real ApplicAtion	Ref.
Au/PEGDA/vFc/GOx	amperometry	0–0.6	first generation	-	[51]
Au/FcCOOH/GOx	amperometry	2–13.5	first generation	-	[52]
C/CMC/GOx	amperometry	0–35	self-powered	-	[21]
AuNPs-PtNPs/PANI/PtNPs/ GOx/PVDF-Naf	amperometry	0–20	first generation	in vivo	[53]
Au/MPA/GOx	Cyclic voltammetry	2.8–22.2	first generation	in vitro	[54]
Au/PP/GOx	amperometry	-	first generation	in vivo	[5]
CP/GOx/TTF-CP/Pt black	polarization curve	0–25	self-powered	-	[19]
Au/pTCA-GOx	amperometry	0.05–20	first generation	-	[55]
GDH/pMB/AuMWCNTs/Au	amperometry	0.05–5	second generation	-	[23]
FAD-GDH/FcSH/h-PG/Au	amperometry	0.1–10	second generation	-	this work

List of abbreviations: MPA, 3-mercaptopropionic acid; PVDF, three-dimensional (3D) porous polyvinylidene fluoride; C, carbon-based electrode; CP, carbon paste; CMC, carboxymethyl cellulose; PP, electropolymerized polyphenol; FAD-GDH, FAD-glucose dehydrogenase; FcCOOH, ferrocene monocarboxylic acid; GOx, glucose oxidase; Au, gold electrode; AuNPs, gold nanoparticles; Naf, nafion; Pt black, platinum black; Pt-c, platinum carbon electrode; PtNPs, platinum nanoparticles; PANI, polyaniline; PEGDA, polyethylene glycol diacrylate; TTF, tetrathiafulvalene; vFc, vinylferrocene; BSA, bovine serum albumin; GA, glutaraldehyde; TCA, terthiophene carboxylic acid; pMB, polymethylenblue.

2.5. Simulation of Continuous Glucose Monitoring Using a Skin Model

The feasibility of the FcSH/h-PG/Au microneedles-based biosensor for continuous glucose monitoring was tested in flow conditions for 12 h through the determination of the glucose concentrations in a skin model, consisting of a chitosan/agarose hydrogel opportunely embedded in artificial ISF at two different glucose concentrations, 4 mM and 8 mM, in order to simulate the normal glucose levels in a healthy patient under fasting conditions (in the morning before breakfast) and after lunch (approximately 6 h after breakfast). Both current signals presented a lag-time of about 2 min compared to the experiments performed in solution, possibly because of the time of diffusion of

glucose through the hydrogel; the signals resulted to be quite stable, thus attesting to the robustness of the developed device. The current signal registered for the 8 mM glucose concentration resulted to be about 2 times higher than that registered at the 4 mM glucose concentration, confirming that the two concentrations fall perfectly into the linearity range of the glucose biosensor (0.1–10 mM).

3. Materials and Methods

3.1. Reagents and Apparatus

3-(N-morpholino)propanesulfonic acid (MOPS), 4-(2-Hydroxyethyl)piperazine-1-ethanesulfonic acid (HEPES), ammonium chloride (NH_4Cl), ascorbic acid (AA), boric acid, calcium chloride ($CaCl_2$), D-(−)-glucose (Glc), ferricynide ($Fe(CN)_6^{3-}$), ferrocyanide ($Fe(CN)_6^{4-}$), magnesium sulfate ($MgSO_4$), 6-(ferrocenyl)hexanethiol (FcSH), potassium chloride (KCl), potassium nitrate (KNO_3), saccharose, agarose, chitosan with medium molecular weight, sodium acetate (CH_3COONa), sodium tetraborate, sodium chloride (NaCl) sodium L-lactate, sodium phosphate dibasic (Na_2HPO_4), sodium phosphate monobasic (NaH_2PO_4), sulfuric acid (H_2SO_4), hydrochloric acid (HCl), tris(hydroxymethyl)aminomethane (TRIS), uric acid (UA), D-fructose, D-galactose, D-mannitol, and tetrachloauric acid ($HAuCl_4$) were purchased from Sigma Aldrich (St. Louis, MO, USA).

FAD-glucose dehydrogenase (FAD-GDH) from *Aspergillus niger* was obtained from Creative Enzyme Ltd. The FAD-GDH (activity 300 U/mL) was solubilized in a 10 mM PBS buffer (pH 7.5) and stored at −20 °C until further use.

To prepare the artificial interstitial fluid (ISF), 2.5 mM $CaCl_2$, 10mM Hepes, 3.5 mM KCl, 0.7 mM $MgSO_4$, 123 mM NaCl, 1.5 mM NaH_2PO_4, 7.4 mM saccharose were mixed, and the solution was adjusted to pH 7.5. Milli-Q water (18.2 MΩ cm, Millipore, Bedford, MA, USA) was used to prepare all solutions.

All electrochemical experiments were performed using a PGSAT204N potentiostat (Eco Chemie, The Netherlands) equipped with Nova 2.1 software (Eco Chemie, The Netherlands). All potentials are referred to a saturated calomel electrode (SCE, 244 mV vs. NHE, Cat. 303/SCG/12, AMEL, Milano, Italy). Moreover, gold planar- or microneedle-based electrodes and a glassy carbon rod electrode (d = 2 mm, Cat. 6.1241.020, Metrohm, Herisau, Switzerland) were employed as working and counter electrodes, respectively. The temperature was controlled using a thermostatic bath (T ± 0.01 °C, LAUDA RM6, Delran, NJ, USA).

The morphology of the electrodes was investigated by using High-Resolution Field Emission Scanning Electron Microscopy (SEM) (HR FESEM, Zeiss Auriga Microscopy, Jena, Germany). All samples were prepared using gold slides (25 Å~ 25 Å~ 1 mm, ALS Co. Ltd., Tokyo, Japan) and microneedles electrodes.

3.2. Modification of Au Microneedles-Based Electrode

The microneedles-array Au microneedles electrodes were kindly provided by a collaborator at Glasgow University [25,43]. These electrodes are based on a polycarbonate scaffold (0.5 × 0.5 × 0.02 cm) with 64 microneedles divided as four 4 × 4 arrays. Each pyramid showed the following dimensions: base 0.06 cm; height 0.1 cm; 4 × 4 array area 0.2 cm^2. On this platform, three electrodes were used as working electrodes (gold), while the fourth electrode was the reference electrode (silver). However, in the present work, we used an external saturated calomel electrode as a reference electrode to run the preliminary experiments.

At the beginning, the microneedles electrodes were electrochemically cleaned by sweeping the potential between −0.3 and 1.7 V versus SCE 20 times at a scan rate of 300 mV s^{-1} in 0.5 M H_2SO_4. The electrodeposition of highly porous gold (h-PG) was performed by cycling the potential between +0.8 and 0 V versus SCE for 25 scans at 50 mV s^{-1} in a solution containing 10 mM $HAuCl_3$ and 2.5 M NH_4Cl. Afterwards, a fixed potential of −2 V versus SCE was applied in the same solution in order to activate the self-templated formation of pores. Next, the electrodes were activated in 0.5 M

H_2SO_4 by running CVs between 0 and +1.7 V versus SCE at a scan rate of 100 mV s^{-1} for 25 cycles. All the electrochemical parameters (e.g., electroactive surface area, heterogeneous electron transfer rate constant (k^0, cm s^{-1}), and roughness factor (ρ)) were obtained in 5 mM $Fe(CN)_6^{3-/4-}$ (50 mM PBS buffer pH 7.5 + 137 mM NaCl). Furthermore, the as-prepared h-PG/Au microneedles electrode was modified through self-assembling monolayer formation by incubating the electrode in an 8 mM FcSH solution overnight. After thoroughly washing the electrode with working buffer, 5 µL of FAD-GDH enzyme were cast onto the modified electrode.

3.3. Modification of Au Planar Electrode

Planar gold electrodes (AuE) (d = 1.6 mm, AMEL, Milano, ITALY) were carefully cleaned with Piranha solution (1:3 mixture of conc. H_2O_2 with H_2SO_4, *CAUTION: Piranha solution is especially dangerous, corrosive and may explode if contained in a closed vessel, it should be handled with special care*). Afterwards, they were mechanically cleaned with polishing cloths and deagglomerated alumina slurry of 1 µm in diameter (SIEM, Bologna, ITALY), and successively sonicated in ultrapure water for 5 min. Next, the electrodes were electrochemically cleaned by sweeping the potential in the range between −0.3 and 1.7 V versus SCE at a scan rate of 300 mV s^{-1} M for 20 cycles in 0.5 M H_2SO_4. The h-PG surface was realized by a self-templating method, as reported above. The as-modified electrodes were characterized and modified following the microneedles protocol reported in the previous section.

4. Conclusions

In this work, we described the fabrication and characterization of a novel glucose biosensor based on microneedles technology. The novelty of the work consists in the realization of a h-PG gold microneedles electrode and in the use of the mediator 6-(ferrocenyl)hexanethiol, thus realizing a second-generation biosensor with improved performance in terms of linear range, sensitivity, and selectivity. The highly porous film was electrochemically fabricated through a deposition/self-templating method that made the active surface area of the microneedles electrode up to 100 times larger than that of a classical bare one, thus enhancing the sensitivity of the biosensor. The device was tested in artificial interstitial fluid, showing good repeatability and good long-term stability, and also under simulated continuous monitoring conditions in a chitosan/agarose hydrogel skin model. The obtained results are encouraging for the use of the proposed microneedles-based biosensor as a wearable device to be used in medicine for the continuous monitoring of glucose in patients with diabetes. Investigation of in vivo performance through experiments in healthy and diabetic volunteers will be the next aim of the work. Further work will be devoted also to the realization of toxicity tests of the developed device, on the one hand, as well as to studies of a possible integration of suitable electronics for wireless communication, on the other hand.

Supplementary Materials: The following are available online at http://www.mdpi.com/2073-4344/9/7/580/s1, Figure S1: Effect of enzyme loading on biosensor response, Table S1: Heterogeneous electron transfer rate constant (k0), real electroactive area (AEA), and roughness factor (ρ) of a gold planar electrode and a gold microneedles-based electrode before and after the electrodeposition of h-PG and Au-MWCNTs.

Author Contributions: Investigation: P.B.; Resources: S.S., A.E.G.C.; Supervision: F.T.; Writing original draft: R.A.

Acknowledgments: This work was supported by Italian Ministry of Education, Universities and Research Dipartimenti di Eccellenza, L. 232/2016.

Conflicts of Interest: The authors declare no conflicts of interest.

References

1. Wild, S.; Roglic, G.; Green, A.; Sicree, R.; King, H. Global prevalence of diabetes: estimates for the year 2000 and projections for 2030. *Diabetes Care* **2004**, *27*, 1047–1053. [CrossRef] [PubMed]
2. Shaw, J.E.; Sicree, R.A.; Zimmet, P.Z. Global estimates of the prevalence of diabetes for 2010 and 2030. *Diabetes Res. Clin. Pract.* **2010**, *87*, 4–14. [CrossRef] [PubMed]

3. O'Kane, M.J.; Pickup, J. Self-monitoring of blood glucose in diabetes: Is it worth it? *Ann. Clin. Biochem.* **2009**, *46*, 273–282. [CrossRef] [PubMed]
4. Oliver, N.; Toumazou, C.; Cass, A.; Johnston, D. Glucose sensors: A review of current and emerging technology. *Diabetic Med.* **2009**, *26*, 197–210. [CrossRef] [PubMed]
5. Sharma, S.; Huang, Z.; Rogers, M.; Boutelle, M.; Cass, A.E. Evaluation of a minimally invasive glucose biosensor for continuous tissue monitoring. *Anal. Bioanal. Chem.* **2016**, *408*, 8427–8435. [CrossRef] [PubMed]
6. Pickup, J.C.; Freeman, S.C.; Sutton, A.J. Glycaemic control in type 1 diabetes during real time continuous glucose monitoring compared with self monitoring of blood glucose: meta-analysis of randomised controlled trials using individual patient data. *Br. Med. J.* **2011**, *343*, d3805. [CrossRef]
7. Chinnadayyala, S.R.; Park, K.D.; Cho, S. Editors' Choice—Review—In Vivo and In Vitro Microneedle Based Enzymatic and Non-Enzymatic Continuous Glucose Monitoring Biosensors. *ECS J. Solid State Sci. Technol.* **2018**, *7*, Q3159–Q3171. [CrossRef]
8. Paliwal, S.; Hwang, B.H.; Tsai, K.Y.; Mitragotri, S. Diagnostic opportunities based on skin biomarkers. *Eur. J. Pharm. Sci.* **2013**, *50*, 546–556. [CrossRef]
9. Sharma, S.; Saeed, A.; Johnson, C.; Gadegaard, N.; Cass, A.E. Rapid, low cost prototyping of transdermal devices for personal healthcare monitoring. *Sens. Biosens. Res.* **2017**, *13*, 104–108. [CrossRef]
10. Ventrelli, L.; Marsilio Strambini, L.; Barillaro, G. Microneedles for transdermal biosensing: current picture and future direction. *Adv. Healthcare Mater.* **2015**, *4*, 2606–2640. [CrossRef]
11. Miller, P.R.; Narayan, R.J.; Polsky, R.J. Microneedle-based sensors for medical diagnosis. *J. Mater. Chem. B.* **2016**, *4*, 1379–1383. [CrossRef]
12. Windmiller, J.R.; Zhou, N.; Chuang, M.-C.; Valdés-Ramírez, G.; Santhosh, P.; Miller, P.R.; Narayan, R.; Wang, J. Microneedle array-based carbon paste amperometric sensors and biosensors. *Analyst* **2011**, *136*, 1846–1851. [CrossRef] [PubMed]
13. Hwa, K.-Y.; Subramani, B.; Chang, P.-W.; Chien, M.; Huang, J.-T. Transdermal microneedle array-based sensor for real time continuous glucose monitoring. *Int. J. Electrochem. Sci* **2015**, *10*, 2455–2466.
14. El-Laboudi, A.; Oliver, N.S.; Cass, A.; Johnston, D. Use of microneedle array devices for continuous glucose monitoring: A review. *Diabetes Technol. Ther.* **2013**, *15*, 101–115. [CrossRef] [PubMed]
15. Gerstel, M.S.; Place, V.A. Drug delivery device. Google Patents US3964482A, 22 June 1976.
16. Henry, S.; McAllister, D.V.; Allen, M.G.; Prausnitz, M.R. Microfabricated microneedles: A novel approach to transdermal drug delivery. *J. Pharm. Sci.* **1998**, *87*, 922–925. [CrossRef] [PubMed]
17. Kim, Y.-C.; Park, J.-H.; Prausnitz, M.R. Microneedles for drug and vaccine delivery. *Adv. Drug Delivery Rev.* **2012**, *64*, 1547–1568. [CrossRef] [PubMed]
18. Valdés-Ramírez, G.; Li, Y.-C.; Kim, J.; Jia, W.; Bandodkar, A.J.; Nuñez-Flores, R.; Miller, P.R.; Wu, S.-Y.; Narayan, R.; Windmiller, J.R. Microneedle-based self-powered glucose sensor. *Electrochem. Commun.* **2014**, *47*, 58–62. [CrossRef]
19. Bhatnagar, S.; Dave, K.; Venuganti, V.V.K. Microneedles in the clinic. *J. Controlled Release.* **2017**, *260*, 164–182. [CrossRef]
20. Strambini, L.; Longo, A.; Scarano, S.; Prescimone, T.; Palchetti, I.; Minunni, M.; Giannessi, D.; Barillaro, G. Self-powered microneedle-based biosensors for pain-free high-accuracy measurement of glycaemia in interstitial fluid. *Biosens. Bioelectron.* **2015**, *66*, 162–168. [CrossRef]
21. Stout, P.J.; Peled, N.; Erickson, B.J.; Hilgers, M.E.; Racchini, J.R.; Hoegh, T.B. Comparison of glucose levels in dermal interstitial fluid and finger capillary blood. *Diabetes Technol. Ther.* **2011**, *3*, 81–90. [CrossRef]
22. Boyne, M.S.; Silver, D.M.; Kaplan, J.; Saudek, C.D. Timing of changes in interstitial and venous blood glucose measured with a continuous subcutaneous glucose sensor. *Diabetes* **2003**, *52*, 2790–2794. [CrossRef] [PubMed]
23. Bollella, P.; Sharma, S.; Cass, A.E.G.; Antiochia, R. Minimally-invasive Microneedle-based Biosensor Array for Simultaneous Lactate and Glucose Monitoring in Artificial Interstitial Fluid. *Electroanalysis* **2019**, *31*, 374–382. [CrossRef]
24. Jina, A.; Tierney, M.J.; Tamada, J.A.; McGill, S.; Desai, S.; Chua, B.; Chang, A.; Christiansen, M.J. Design, development, and evaluation of a novel microneedle array-based continuous glucose monitor. *J. Diabetes Sci. Technol.* **2014**, *8*, 483–487. [CrossRef] [PubMed]
25. Sharma, S.; Takagi, E.; Cass, T.; Tsugawa, W.; Sode, K. Minimally invasive microneedle array electrodes employing direct electron transfer type glucose dehydrogenase for the development of continuous glucose monitoring sensors. *Procedia Technol.* **2017**, *27*, 208–209. [CrossRef]

26. Caliò, A.; Dardano, P.; Di Palma, V.; Bevilacqua, M.; Di Matteo, A.; Iuele, H.; De Stefano, L. Polymeric microneedles based enzymatic electrodes for electrochemical biosensing of glucose and lactic acid. *Sens. Actuators B* **2016**, *236*, 343–349. [CrossRef]
27. Miller, P.R.; Skoog, S.A.; Edwards, T.L.; Lopez, D.M.; Wheeler, D.R.; Arango, D.C.; Xiao, X.; Brozik, S.M.; Wang, J.; Polsky, R. Multiplexed microneedle-based biosensor array for characterization of metabolic acidosis. *Talanta* **2012**, *88*, 739–742. [CrossRef] [PubMed]
28. Bollella, P.; Sharma, S.; Cass, A.E.G.; Antiochia, R. Microneedle-based biosensor for minimally-invasive lactate detection. *Biosens. Bioelectron.* **2019**, *123*, 152–159. [CrossRef] [PubMed]
29. Mohan, A.V.; Windmiller, J.R.; Mishra, R.K.; Wang, J. Continuous minimally-invasive alcohol monitoring using microneedle sensor arrays. *Biosens. Bioelectron.* **2017**, *91*, 574–579. [CrossRef]
30. Rawson, T.M.; Sharma, S.; Georgiou, P.; Holmes, A.; Cass, A.; O'Hare, D. Towards a minimally invasive device for beta-lactam monitoring in humans. *Electrochem. Commun.* **2017**, *82*, 1–5. [CrossRef]
31. Windmiller, J.R.; Valdés-Ramírez, G.; Zhou, N.; Zhou, M.; Miller, P.R.; Jin, C.; Brozik, S.M.; Polsky, R.; Katz, E.; Narayan, R. Bicomponent Microneedle Array Biosensor for Minimally-Invasive Glutamate Monitoring. *Electroanalysis* **2011**, *23*, 2302–2309. [CrossRef]
32. Abrar, M.A.; Dong, Y.; Lee, P.K.; Kim, W.S. Bendable electro-chemical lactate sensor printed with silver nano-particles. *Sci. Rep.* **2016**, *6*, 30565. [CrossRef] [PubMed]
33. Bollella, P.; Gorton, L. Enzyme based amperometric biosensors. *Curr. Opin. Electrochem.* **2018**, *10*, 157–173. [CrossRef]
34. Karadag, M.; Geyik, C.; Demirkol, D.O.; Ertas, F.N.; Timur, S. Modified gold surfaces by 6-(ferrocenyl) hexanethiol/dendrimer/gold nanoparticles as a platform for the mediated biosensing applications. *Mater. Sci. Eng. C* **2013**, *33*, 634–640. [CrossRef] [PubMed]
35. Baldo, T.A.; Seraphim, P.M.; Gomes, H.M.; Teixeira, M.F. Glucose Biosensor Based on the Hexacyanoferrate 11-Mercaptoundecyl-N′, N″, N‴-Trimethylammonium/6-(Ferrocenyl) Hexanethiol. *Procedia Eng.* **2014**, *87*, 300–303. [CrossRef]
36. Antiochia, R.; Lavagnini, I.; Magno, F. Electrocatalytic oxidation of dihydronicotinamide adenine dinucleotide with ferrocene carboxylic acid by diaphorase from Clostridium kluveri. Remarks on the kinetic approaches usually adopted. *Electroanalysis* **1999**, *11*, 129–133. [CrossRef]
37. Zhang, R.; Olin, H. Porous gold films—A short review on recent progress. *Materials* **2014**, *7*, 3834–3854. [CrossRef] [PubMed]
38. Bollella, P.; Hibino, Y.; Kano, K.; Gorton, L.; Antiochia, R. Highly Sensitive Membraneless Fructose Biosensor Based on Fructose Dehydrogenase Immobilized onto Aryl Thiol Modified Highly Porous Gold Electrode: Characterization and Application in Food Samples. *Anal. Chem.* **2018**, *90*, 12131–12136. [CrossRef]
39. Deng, Y.; Huang, W.; Chen, X.; Li, Z. Facile fabrication of nanoporous gold film electrodes. *Electrochem. Commun.* **2008**, *10*, 810–813. [CrossRef]
40. Ben-Ali, S.; Cook, D.A.; Evans, S.A.; Thienpont, A.; Bartlett, P.N.; Kuhn, A. Electrocatalysis with monolayer modified highly organized macroporous electrodes. *Electrochem. Commun.* **2003**, *5*, 747–751. [CrossRef]
41. Plowman, B.J.; Jones, L.A.; Bhargava, S.K. Building with bubbles: The formation of high surface area honeycomb-like films via hydrogen bubble templated electrodeposition. *Chem. Comm.* **2015**, *51*, 4331–4346. [CrossRef]
42. Sanzó, G.; Taurino, L.; Antiochia, R.; Gorton, L.; Favero, G.; Mazzei, F.; De Micheli, G.; Carrara, S. Bubble electrodeposition of gold porous nanocorals for the enzymatic and non-enzymatic detection of glucose. *Bioelectrochemistry* **2016**, *112*, 125–131. [CrossRef] [PubMed]
43. Cass, A.E.; Sharma, S. Microneedle enzyme sensor arrays for continuous in vivo monitoring. *Methods Enzymol.* **2017**, *589*, 413–427. [PubMed]
44. Wannapob, R.; Thavarungkul, P.; Dawan, S.; Numnuam, A.; Limbut, W.; Kanatharana, P. A Simple and Highly Stable Porous Gold-based Electrochemical Sensor for Bisphenol A Detection. *Electroanalysis* **2017**, *29*, 472–480. [CrossRef]
45. Lavagnini, I.; Antiochia, R.; Magno, F. An extended method for the practical evaluation of the standard rate constant from cyclic voltammetric data. *Electroanalysis* **2004**, *16*, 505–506. [CrossRef]
46. Lavagnini, I.; Antiochia, R.; Magno, F. A Calibration-Base Method for the Evaluation of the Detection Limit of an Electrochemical Biosensor. *Electroanalysis* **2007**, *19*, 1227–1230. [CrossRef]

47. Creager, S.E.; Rowe, G.K. Redox properties of ferrocenylalkane thiols coadsorbed with linear n-alkanethiols on polycrystalline bulk gold electrodes. *Anal. Chim. Acta* **1991**, *246*, 233–239. [CrossRef]
48. Belding, S.R.; Campbell, F.W.; Dickinson, E.J.; Compton, R.G. Nanoparticle-modified electrodes. *Phys. Chem. Chem. Phys.* **2010**, *12*, 11208–11221. [CrossRef]
49. Menshykau, D.; Streeter, I.; Compton, R.G. Influence of electrode roughness on cyclic voltammetry. *J. Phys. Chem. C* **2008**, *112*, 14428–14438. [CrossRef]
50. Ferri, S.; Kojima, K.; Sode, K. Review of glucose oxidases and glucose dehydrogenases: a bird's eye view of glucose sensing enzymes. *J. Diabetes Sci. Technol.* **2011**, *5*, 1068–1076. [CrossRef]
51. Dardano, P.; Caliò, A.; Di Palma, V.; Bevilacqua, M.; Di Matteo, A.; De Stefano, L. Glucose sensing electrode system based on polymeric microneedles. In Proceedings of the IEEE Sensors Appl. Symposium (SAS), Catania, Italy, 20–22 April 2016.
52. Barrett, C.; Dawson, K.; O'Mahony, C.; O'Riordan, A. Development of low cost rapid fabrication of sharp polymer microneedles for in vivo glucose biosensing applications. *ECS J. Solid State Sci. Technol.* **2015**, *4*, S3053–S3058. [CrossRef]
53. Chen, D.; Wang, C.; Chen, W.; Chen, Y.; Zhang, J.X. PVDF-Nafion nanomembranes coated microneedles for in vivo transcutaneous implantable glucose sensing. *Biosens. Bioelectron.* **2015**, *74*, 1047–1052. [CrossRef] [PubMed]
54. Lee, H.; Hong, Y.J.; Baik, S.; Hyeon, T.; Kim, D.H. Enzyme-based glucose sensor: from invasive to wearable device. *Adv. Healthcare Mater.* **2018**, *7*, 17011. [CrossRef] [PubMed]
55. Kim, K.B.; Lee, W.C.; Cho, C.H.; Park, D.S.; Cho, S.J.; Shim, Y.B. Continuous glucose monitoring using a microneedle array sensor coupled with a wireless signal transmitter. *Sens. Actuators B* **2019**, *281*, 14–21. [CrossRef]
56. Tasca, F.; Tortolini, C.; Bollella, P.; Antiochia, R. Microneedle-based electrochemical devices for transdermal biosensing: A review. *Curr. Opin. Electrochem.* **2019**, *16*, 42–49. [CrossRef]